A new strain fracture criterion for bulk metallic glasses under complex compressive loading

Li Yu , Tzu-Chiang Wang

PII: S0020-7683(18)30394-9
DOI: https://doi.org/10.1016/j.ijsolstr.2018.09.030
Reference: SAS 10134

To appear in: *International Journal of Solids and Structures*

Received date: 23 May 2018
Revised date: 30 August 2018
Accepted date: 27 September 2018

Please cite this article as: Li Yu , Tzu-Chiang Wang , A new strain fracture criterion for bulk metallic glasses under complex compressive loading, *International Journal of Solids and Structures* (2018), doi: https://doi.org/10.1016/j.ijsolstr.2018.09.030

A new strain fracture criterion for bulk metallic glasses under complex compressive loading

Li Yu[1,2], Tzu-Chiang Wang[1,2*]

[1]*State Key Laboratory of Nonlinear Mechanics, Institute of Mechanics, Chinese Academy of Sciences, Beijing 100190, China.*

[2]*School of Engineering Sciences, University of Chinese Academy of Sciences, Beijing 100049, China*

Correspondence and requests for materials should be addressed to: Tzu-Chiang Wang (email: tcwang@imech.ac.cn)

Abstract: The existing fracture criteria for bulk metallic glasses (BMGs) are described by the stress state on fracture plane. However, they are incapable to predict the fracture behavior of BMGs under compression loading because the nominal stress of most BMGs remains unchanged once materials yield. In this study, a new strain fracture criterion for bulk metallic glasses under complex compressive loading is proposed. The yield and plastic deformation before fracture under compression loading are described by the Drucker-Prager (D-P) criterion and plastic normality rule. Furthermore, due to the elastic perfect–plastic behavior of nominal stress for BMGs, we choose the nominal stress to describe the D-P yield criterion, which is well coincident with the experimental results. The two typical BMGs of $Zr_{52.5}Cu_{17.9}Ni_{14.6}Al_{10}Ti_5$ (Vit105) and $Zr_{41.2}Ti_{13.8}Cu_{12.5}Ni_{10.0}Be_{22.5}$ (Vit1) are used as examples to analyze the fracture behavior of BMGs under complex compressive loading. In this case, the plastic behavior of BMGs depends on the deformation modes, and the results can well describe the increasing tendency of plastic deformation to the higher pressure.

Key words: strain fracture criterion; confining pressure effects; metallic glasses; compressive plastic behavior

1. Introduction

As a relatively new class of materials, BMGs have been extensively explored for about half of a century, showing promising potential for engineering applications due to its mechanical, physical and chemical properties (Greer, 1995; Inoue, 2000; Johnson, 1986; Schuh et al., 2007). In particular, their mechanical behaviors and properties are different from other traditional metal materials, which arise great scientific interests. Generally speaking, BMGs have ultrahigh strength which is close to the theoretical limit (Greer, 1995) due to the absence of crystal slip mechanisms in BMGs, and the pressure- or normal stress-dependence mechanical response gives rise to the tension-compression asymmetry, as well as differences in fracture strength and angle under different loading modes. (Caris and Lewandowski, 2010; Davis and Kavesh, 1975; Donovan, 1988; Lewandowski and Lowhaphandu, 2002; Liu et al., 1998).

Due to the application prospect of BMGs, a lot of efforts are dedicated to investigate the fracture behavior of BMGs (Lei et al., 2015a; Lei et al., 2015b; Wang et al., 2013; Zhang et al., 2003). Meanwhile, many yield and fracture criteria were proposed to provide reference for the safety of BMGs, such as Mohr-Coulomb (M-C) criterion (Schuh and Lund, 2003; Yu, 2002), ellipse criterion (Qu et al., 2011; Zhang and Eckert, 2005), stress hyperbola criterion (Qu and Zhang, 2013), and eccentric ellipse criterion (Chen et al., 2011). All of these criteria focus on the pressure-dependence mechanical of BMGs, while ignoring another feature (elastic perfectly-plastic) of many metallic glasses (Bruck et al., 1994; Hufnagel et al., 2002; Schroers and Johnson, 2004).

Since the BMGs have been discovered, their macroscopic plasticity is limited or even negligible for a long time. (Chen et al., 1994; Flores and Dauskardt, 1999; Hays et al., 2000; Steif et al., 1982; Xing et al., 2001). Yet, some novel BMGs developed in

the last two decades have overcome this barrier by often showing extreme macroscopic compressive plasticity along with considerably high yield strength. There are many factors and ideas have been found to improve and understand the ductility of BMGs, such as the composition of BMGs (Das et al., 2005; Hays et al., 2000; Park and Kim, 2006; Schroers and Johnson, 2004; Yang et al., 2014), Electrodeposition (Ren et al., 2015), and atomic scale effects (Sarac et al., 2018), etc. The disadvantage of its poor plasticity is expected to be thoroughly improved in the future applications. Furthermore, experiments of BMGs under multi-axial loading also show the macroscopical plastic behaviors of BMGs that are closely related to the loading conditions. With the increasing of superimposed confining pressure, the specimens of BMGs display greater macroscopic plasticity before failure (Caris and Lewandowski, 2010; Lu and Ravichandran, 2003). These phenomena indicate the plasticity of BMGs may not be ignored in the future. In this case, due to the elastic perfectly-plastic behavior of most BMGs, the nominal stress remains unchanged once the material yields, and the Cauchy stress decreases as the cross-sectional area increases. The existing fracture criteria described by stress are unable to predict the fracture behavior of BMGs. Furthermore, Materials usually suffer complex stress loading in engineering application, and the existing fracture criteria always limited to the study of simple loading. They not only fail to explain the change of the plasticity of the BMGs under different loading conditions, but also cannot describe the great plasticity of the new BMGs. Thus, the suitable compression fracture criterion and analysis method for BMGs under complex loading thus become quite essential.

In this paper, we aim to propose a criterion that is more suitable for describing the fracture behavior of BMGs under complex compression loading. The strain state at fracture plane is considered to describe the fracture of BMGs. Based on the previous researches, we propose a new strain hyperbola fracture criterion for BMGs under compressive loading. In order to verify the new fracture criterion, the fracture behaviors of two typical Zr-based BMGs under complex loading are discussed. The

results show that the plasticity of BMGs is affected by both the loading conditions and its intrinsic properties, which is consistent with the experimental phenomena.

2. Theory

To explore the fracture behavior and criteria of BMGs under complex compressive loading, we consider a round compressive bar under superimposed confining pressure as shown in Fig. 1(a). The superimposed confining pressure is proportional to the axial tensile stress, and the stress state can be expressed as $S_{22}=S_{33}=\rho S_{11}\left(S_{11}<0\right)$, where S_{ii} is the nominal stress in x_i-axis, and ρ is the proportionality coefficient between the axial stress and confining pressure. Due to the symmetry of round bar, we consider that the normal of the fracture plane (x_1^*-axis) locates at the x_1-x_3 plane as shown in Fig.1 (b).

It can be noticed that the radial load on the round bar is tensile stress when $\rho<0$, and ρ with high value represents high triaxial pressure. Both of two cases are rare in mechanical experimental and engineering application. Thereby, we choose an appropriate range ($-0.1<\rho<0.6$) of ρ to analyze the fracture behavior of BMGs. In order to fully understand the change of ρ near 0, thus, we choose -0.1 as the lower limit of ρ.

2.1 Fracture criterion

BMGs usually display elastic perfectly-plastic deformation behavior under uniaxial compression. The nominal stress remains unchanged once the material yields, and Cauchy stress decreases as the cross-sectional area increases. In this case, the criterion described by stress state is no longer suitable to describe the fracture behavior of BMGs. Moreover, the strain of BMGs continuously increase before material failure. The damage can always be expressed by the strain state. Thus the strain state of BMGs is more suitable to describe its fracture behavior. The general

form of fracture criterion F can be expressed as

$$F\left(\varepsilon,\gamma/2\right)=0, \tag{1}$$

where $\gamma/2$ is the shear strain at the fracture plane which is main factor leading to fracture, ε is the normal strain at the fracture plane to reflect the pressure sensitivity of BMGs. In order to study the fracture behavior under complex loading, it is necessary to know the fracture angle under different loading conditions, which can be obtained by the similar method in our previous study (Yu and Wang, 2017). It provides a universal formula which considers the most dangerous plane can be found by seeking the tangency of fracture lines. This formula can be rewritten by a strain form as

$$tg\left(2\theta\right)=-\frac{\partial F/\partial\left(\gamma/2\right)}{\partial F/\partial\varepsilon}. \tag{2}$$

Eq. (2) indicates that the fracture angle is related to the first-order derivate of the function F. It is worth noting that the pure shear experiment (Chen et al., 2016) shows that the fracture in BMGs occurs along the pure shear plane (corresponding to a fracture angle of 45°), which is different from its uniaxial compressive fracture angle 42°. It indicates that the fracture angle of BMGs depends on the fracture mode.

Expanded from the ellipse criterion for tension loading, the stress hyperbola criterion was proposed to predict compression failure of BMGs (Qu and Zhang, 2013), which is expressed by the second-order equation of normal and shear stress at the fracture plane. Thus, we propose a strain hyperbola fracture criterion for compression loading as below

$$\left(\frac{\gamma}{2}\right)^2-\alpha_C^2\varepsilon^2=\left(\frac{\gamma_{Cf}}{2}\right)^2, \tag{3}$$

where α_C is an intrinsic parameter to describe the pressure sensitivity in different disordered solids, and γ_{Cf} represents the critical shear strain which describes the ability to resist shear deformation of the materials. The γ_{Cf} is related to deformation

mode, which can be approximately expressed as

$$\gamma_{Cf} = \gamma_{C0}\left[1+\beta\left(1+\rho'\right)\right], \tag{4}$$

where $\rho' = \varepsilon_3 / \varepsilon_1$ is a parameter to characterize the deformation state, ε_1 and ε_3 are fracture strain along x_1 and x_3, respectively. The γ_{C0} is the critical pure shear strain of the BMGs and β is a material constant.

Figure. 2 shows the positional relationship between fracture lines and critical Mohr circles when pure shear strain ($\rho' = -1$) and general cases. For a given deformation state ($\varepsilon, \gamma/2$), its corresponding fracture angle θ can be obtained by Eq. (2),

$$tg(2\theta) = -\frac{\gamma}{2\alpha_C^2 \varepsilon}. \tag{5}$$

By applying the strain fracture criterion to predict the fracture properties under uniaxial compression and pure shear loading, the materials constants α_C, β can be derived as

$$\alpha_C = \sqrt{\frac{\chi_{uni}\cos\left(2\theta_{uni}\right)}{1-\chi_{uni}\cos\left(2\theta_{uni}\right)}}, \tag{6}$$

$$\beta = \frac{\varepsilon_{uni}^2\left(1-\rho'_{uni}\right)}{\gamma_{C0}}\left[\chi_{uni}-\cos\left(2\theta_{uni}\right)\right]-\frac{1}{1+\rho'_{uni}}, \tag{7}$$

where $\chi_{uni} = \left(1-\rho'_{uni}\right)/\left(1+\rho'_{uni}\right)$, and ρ'_{uni} represents the deformation mode under uniaxial compression. The ε_{uni} and θ_{uni} are the uniaxial fracture strain and angle respectively. Moreover, the pure shear critical strain γ_{C0} can be expressed as

$$\gamma_{C0} = \tau_0 / G, \tag{8}$$

where τ_0 is the pure shear fracture strength. According to equations(5)-(7), the three material constants α_C, γ_{C0} and β of the new failure criterion (Eq. (3)) can be obtained

through uniaxial compression and pure shear experiments.

2.2 Yield criterion and constitutive relation

According to the new fracture criterion, it can be found that the predictions strongly depend on the deformation state. To obtain the complete deformation information, we also need to discuss the yield condition of BMGs. There are several criteria used for BMGs to characterize the yield behavior, such as the traditional von Misses criterion and Drucker-Prager (D-P) criterion which are described by Cauchy stress. In this paper, we choose the nominal stress S_{ij} instead of Cauchy stress to describe yield of BMGs owing to that the Cauchy stress falls down during deformation. The new form can be expressed as

$$f = T_e + \alpha T_m = f_0, \tag{9}$$

where $T_e = \sqrt{T'_{ij}T'_{ij}/2}$ is effective stress, $T'_{ij} = T_{ij} - T_m\delta_{ij}$ is deviatoric stress, $T_m = T_{kk}/3$ is mean stress, and stress tensor $T_{ij} = \left(S_{ij} + S_{ji}\right)/2$. The parameter α represents the pressure sensitivity of yielding and yield strength f_0 represents the material ability to resist yield. The plastic deformation of BMGs obeys the plastic normality rule, thus the relationship between strain rate D_{ij} and stress rate T_{ij} can be written as

$$D_{ij} = \frac{\dot{T}'_{ij}}{2G} + \frac{\dot{T}_m}{K}\delta_{ij} + \dot{\bar{\varepsilon}}_p\left(\frac{T'_{ij}}{2T_e} + \frac{1}{3}\delta_{ij}\alpha\right), \tag{10}$$

where G and K are the elastic shear and bulk modulus respectively. The parameter α in yield criterion can be obtained by complex loading experiments.

Through the constitutive relation in Eq. (10), the relationship between stress rate and strain rate can be obtained after the round bar (Fig. 1)under different loading conditions. We assume that BMGs exhibit elastic perfect-plastic behavior under different loading modes (different ρ). Thus, the nominal stress remains unchanged

once material yielding, and the stress rate $\dot{S}_{11}=\dot{S}_{33}=0$. By combining the loading state into Eq. (10), the plastic strain rate can be obtained by

$$\dot{\varepsilon}_{11}=\dot{\bar{\varepsilon}}_p\left(-\sqrt{3}+\alpha\right)/3, \tag{11}$$

$$\dot{\varepsilon}_{33}=\dot{\bar{\varepsilon}}_p\left(\sqrt{3}/2+\alpha\right)/3. \tag{12}$$

The $\dot{\bar{\varepsilon}}_p$ can be used as a generalized time in calculations. It is interesting to find that the plastic strain rate is independent with the loading condition.

3. The applications of the fracture criterion

3.1 The fracture behaviors of Vit-105 BMG

In order to validate the new criterion (Eq.(3)), we compare the fracture behavior between the theoretical prediction and the experimental results of Zr-based BMG ($Zr_{52.5}Cu_{17.9}Ni_{14.6}Al_{10}Ti_5$,Vit-105) under complex compressive loading. For the Zr-based BMG, the Young's modulus E is 88.6GPa, and Poisson ratio v is 0.37. Its pure shear strength τ_0 is 0.842GPa and the fracture occurs at the maximum shear stress plane (Chen et al., 2016). The fracture under uniaxial compression happens at the strength of $T_{uni}=1.843\text{Gpa}$, and along the fracture angle of $\theta_{uni}=43^{\circ}$ (Qu et al., 2011). Furthermore, the axial compressive fracture strain of Vit-105 is $\varepsilon_{uni}=\varepsilon_1=-5\%$. The corresponding radial strain $\varepsilon_3=2.31\%$ induced by Poisson ratio can be calculated by the constitutive relation Eqs. (11) and (12) with $\alpha=0.03$. Finally, parameters in fracture criterion can be determined with these data as $\alpha_C=0.4836$, $\gamma_{C0}=0.013$, and $\beta=3.2862$.

In terms of the calculated parameters, the fracture curves and corresponding Mohr circles of Vit-105 under different deformation modes are plotted in Fig. 3. With ρ' increasing, the fracture curve moves along the positive direction of $\gamma/2$ axis, which indicates the fracture limit has been improved in this process. Furthermore, the

critical Mohr circle moves along the negative direction of ε axis and grows larger gradually. The red line shows the locus of tangency points, indicating that both the absolute value of normal strain and shear strain increase with ρ' increasing.

More specific results are shown in Fig. 4. On the one hand, the axial and radial plastic strains increase with the increase of ρ (see Fig. 4(a)). Fig. 4(b) also shows the increase trend of the axial elastic strain $|\varepsilon_{11e}|$ (compressive strain). As the confining pressure increase, the radial elastic strain $|\varepsilon_{22e}|$ changes from compressive strain to tensile strain. On the other hand, Fig.4(c) illustrates the dependence between the total fracture strain and the parameter ρ, showing that the total radial strain $|\varepsilon_{22}|$ almost remains constant when the value of ρ is lower than 0.4. Finally, the shear strain $\gamma/2$ along fracture plane is shown in Fig. 4(d). The amount of its change is relatively lager than some other mechanical quantities, which indicates its importance for fracture. These predictions are qualitatively consistent with the experimental results (Caris and Lewandowski, 2010; Lu and Ravichandran, 2003).

Furthermore, the variation of fracture angle with respect to the coefficient ρ is shown in Fig. 5. The fracture angle trends to decrease with the increasing of ρ. The reduction of the fracture angle helps to obtain a larger shear strain at the fracture plane to counter the inhibiting effect of confining pressure on the material failure.

The critical shear strain vs. critical normal strain for Vit-105 is shown in Fig.6**.** The red line is the result for the different deformation modes and the blue points are obtained by different loading modes ($-0.1 \le \rho \le 0.6$). Different loading modes can find corresponding positions on the curve of critical shear strain with critical normal strain.

3.2 Comparisons between the theoretical and experimental results of Vit-1 BMG.

The complex loading experiments for Vit-1 were well performed in the literatures

(Caris and Lewandowski, 2010; Lewandowski and Lowhaphandu, 2002), where the round bars were 12.7 mm in length and 6.35 ± 0.02 mm in diameter, and were subject to the quasi-static compression with superimposed pressure. The superimposed pressure is loaded before the compression begins, which is somewhat different with the proportional loading discussed in this paper. However, due to the elastic perfectly-plastic behavior of BMGs, its nominal fracture stress can be determined directly once the material yields, and the constitutive relationship in elastic deformation of the material is independent of the loading path. Thus, the experimental results of fracture stress can be compared directly with the case of proportional loading.

The variation of the axial fracture stress with respect to ρ according to our theoretical analysis is shown in Fig. 7, and the experimental data is provided for comparisons. It is easy to find that the theoretical calculation results are in good agreement with the experiment data of Vit-1.

4. Discussion

According to the present strain fracture criterion, it can be found that the predictions strongly depend on the parameters α_C and β. The parameter α_C is the intrinsic parameter to reflect the effect of pressure-sensitivity of materials (Qu and Zhang, 2013). The change of plastic fracture strain (uniaxial compression) with β has been shown in Fig. 8, which is obtained by adopting the basic parameters of Vit-105. It can be found that the fracture of BMGs changes from elastic fracture to plastic fracture with the increasing of β, indicating that the parameter β can reflect the intrinsic plasticity of materials. Usually, Materials with low value of β tend to failure without obvious macroscopic plastic deformation. This is why brittle fracture always be observed in some La-based BMGs (Jiang et al., 2007; Wu et al., 2008). For β with higher value, some new BMGs, which are made by introducing a second

crystalline phase into the liquid BMGs or adjusting the proportion of component of BMGs (Choi-Yim and Johnson, 1997; Park and Kim, 2006; Schroers and Johnson, 2004), shows a lager global plasticity under uniaxial compression. Thus, the new fracture criterion not only describes the pressure-sensitivity, but also reflects the plastic deformation ability of different BMGs and makes up for the lack of existing stress criteria.

The mechanical quantities at the fracture plane, such as normal stress and shear stress, are usually used as the basic variables in most fracture criteria, because they possess clear physical significance to fracture. However, the strain state at the fracture plane can be obtained only after the fracture angle is determined, which cannot directly obtained in engineering applications. It can be found that the mean strain and maximum shear strain can reflect the globe shear deformation and bulk strain of material, and they can easily obtained without the fracture angle. Thus, by combining the Eq. (3) and Eq.(5), another representation of the strain fracture criterion can be obtained as following

$$\left(\frac{\gamma_M}{2}\right)^2 - \beta_C^2 \varepsilon_M^2 = \left(\frac{\gamma_{Cf}}{2}\right)^2, \tag{13}$$

where $\beta_C^2 = \alpha_C^2/(1+\alpha_C^2)$, $\gamma_M = (\varepsilon_3 - \varepsilon_1)/2$ and $\varepsilon_M = (\varepsilon_1 + \varepsilon_3)/2$ are the maximum shear strain and the mean strain respectively. As a similar equation of the strain hyperbola fracture criterion, it is more convenient to be applied in engineering applications.

5. Conclusion

In this study, we adopt the strain as the main basic variable for determining the fracture of BMGs. Based on the previous researches, a new hyperbola strain fracture criterion is proposed to describe fracture behavior of BMGs under complex compressive loading. The present strain fracture criterion not only takes the pressure-sensitivity of BMGs into account, but also considers the effect of the

deformation mode and the material characteristics on its plasticity. The different intrinsic plasticity of BMGs can be described by the variation of the intrinsic material constant β. In order to validate this new criterion, we apply it to analyze the fracture behavior of two typical BMGs round bar samples under complex compressive loading. The result of Vit-105 shows that the fracture shear strain and plastic deformation along fracture plane increase with the confining pressure increasing, which agrees with the phenomena in the confining pressure experiments. Through comparing with experiments, it is found that the fracture strength of Vit-1 can be well predicted by the present criterion. For engineering applications, another representation of the strain fracture criterion is also obtained in this paper, which is described by maximum shear strain and mean strain. This new fracture criterion provides a new vision for understanding the fracture mechanisms of various BMGs.

References

Bruck, H.A., Christman, T., Rosakis, A.J., Johnson, W.L., 1994. Quasi-static constitutive behavior of Zr41.25Ti13.75Ni10Cu12.5Be22.5 bulk amorphous alloys. Scripta Metallurgica et Materialia 30, 429-434.

Caris, J., Lewandowski, J.J., 2010. Pressure effects on metallic glasses. Acta Materialia 58, 1026-1036.

Chen, C., Gao, M., Wang, C., Wang, W.-H., Wang, T.-C., 2016. Fracture behaviors under pure shear loading in bulk metallic glasses. Scientific Reports 6, 39522.

Chen, H., He, Y., Shiflet, G.J., Poon, S.J., 1994. Deformation-induced nanocrystal formation in shear bands of amorphous alloys. Nature 367, 541-543.

Chen, Y., Jiang, M.Q., Wei, Y.J., Dai, L.H., 2011. Failure criterion for metallic glasses. Philosophical Magazine 91, 4536-4554.

Choi-Yim, H., Johnson, W.L., 1997. Bulk metallic glass matrix composites. Applied physics letters 71, 3808-3810.

Das, J., Tang, M.B., Kim, K.B., Theissmann, R., Baier, F., Wang, W.H., Eckert, J., 2005. "Work-Hardenable" ductile bulk metallic glass. Physical Review Letters 94, 205501.

Davis, L.A., Kavesh, S., 1975. Deformation and fracture of an amorphous metallic alloy at high pressure. Journal of Materials Science 10, 453-459.

Donovan, P.E., 1988. Compressive deformation of amorphous Pd40Ni40P20. Materials Science and Engineering 98, 487-490.

Flores, K.M., Dauskardt, R.H., 1999. Local heating associated with crack tip plasticity in Zr-Ti-Ni-Cu-Be bulk amorphous metals. Journal of Materials Research 14, 638-643.

Greer, A.L., 1995. Metallic glasses. Science 267, 1947-1953.

Hays, C.C., Kim, C.P., Johnson, W.L., 2000. Microstructure Controlled Shear Band Pattern Formation and Enhanced Plasticity of Bulk Metallic Glasses Containing in situ Formed Ductile Phase Dendrite Dispersions. Physical Review Letters 84, 2901-2904.

Hufnagel, T.C., Jiao, T., Li, Y., Xing, L.Q., Ramesh, K.T., 2002. Deformation and Failure of Zr57Ti5Cu20Ni8Al10 Bulk Metallic Glass Under Quasi-static and Dynamic Compression. Journal of Materials Research 17, 1441-1445.

Inoue, A., 2000. Stabilization of metallic supercooled liquid and bulk amorphous alloys. Acta Materialia 48, 279-306.

Jiang, Q.K., Zhang, G.Q., Yang, L., Wang, X.D., Saksl, K., Franz, H., Wunderlich, R., Fecht, H., Jiang, J.Z., 2007. La-based bulk metallic glasses with critical diameter up to 30mm. Acta Materialia 55, 4409-4418.

Johnson, W.L., 1986. Thermodynamic and kinetic aspects of the crystal to glass transformation in metallic materials. Progress in Materials Science 30, 81-134.

Lei, X., Li, C., Shi, X., Xu, X., Wei, Y., 2015a. Notch strengthening or weakening governed by transition of shear failure to normal mode fracture. Scientific Reports 5, 10537.

Lei, X., Wei, Y., Wei, B., Wang, W.-H., 2015b. Spiral fracture in metallic glasses and its correlation with failure criterion. Acta Materialia 99, 206-212.

Lewandowski, J.J., Lowhaphandu, P., 2002. Effects of hydrostatic pressure on the flow and fracture of a bulk amorphous metal. Philosophical Magazine A 82, 3427-3441.

Liu, C.T., Heatherly, L., Horton, J.A., Easton, D.S., Carmichael, C.A., Wright, J.L., Schneibel, J.H., Yoo, M.H., Chen, C.H., Inoue, A., 1998. Test environments and mechanical properties of Zr-base bulk amorphous alloys. Metallurgical and Materials Transactions A 29, 1811-1820.

Lu, J., Ravichandran, G., 2003. Pressure-dependent flow behavior of Zr41.2Ti13.8Cu12.5Ni10Be22.5 bulk metallic glass. Journal of Materials Research 18, 2039-2049.

Park, E.S., Kim, D.H., 2006. Phase separation and enhancement of plasticity in Cu–Zr–Al–Y bulk metallic glasses. Acta Materialia 54, 2597-2604.

Qu, R.T., Eckert, J., Zhang, Z.F., 2011. Tensile fracture criterion of metallic glass. Journal of Applied Physics 109, 083544.

Qu, R.T., Zhang, Z.F., 2013. A universal fracture criterion for high-strength materials. Scientific Reports 3, 1117.

Ren, L.W., Meng, M.M., Wang, Z., Yang, F.Q., Yang, H.J., Zhang, T., Qiao, J.W., 2015. Enhancement of plasticity in Zr-based bulk metallic glasses electroplated with copper coatings. Intermetallics 57, 121-126.

Sarac, B., Ivanov, Y.P., Chuvilin, A., Schöberl, T., Stoica, M., Zhang, Z., Eckert, J., 2018. Origin of large plasticity and multiscale effects in iron-based metallic glasses. Nature Communications 9, 1333.

Schroers, J., Johnson, W.L., 2004. Ductile bulk metallic glass. Physical Review Letters 93, 255506.

Schuh, C.A., Hufnagel, T.C., Ramamurty, U., 2007. Mechanical behavior of amorphous alloys. Acta Materialia 55, 4067-4109.

Schuh, C.A., Lund, A.C., 2003. Atomistic basis for the plastic yield criterion of metallic glass. Nature Materials 2, 449.

Steif, P.S., Spaepen, F., Hutchinson, J.W., 1982. Strain localization in amorphous metals. Acta

Metallurgica 30, 447-455.

Wang, Z.T., Pan, J., Li, Y., Schuh, C.A., 2013. Densification and Strain Hardening of a Metallic Glass under Tension at Room Temperature. Physical Review Letters 111, 135504.

Wu, W.F., Li, Y., Schuh, C.A., 2008. Strength, plasticity and brittleness of bulk metallic glasses under compression: statistical and geometric effects. Philosophical Magazine 88, 71-89.

Xing, L.Q., Li, Y., Ramesh, K.T., Li, J., Hufnagel, T.C., 2001. Enhanced plastic strain in Zr-based bulk amorphous alloys. Phys.rev.b 64, 607-611.

Yang, W., Liu, H., Zhao, Y., Inoue, A., Jiang, K., Huo, J., Ling, H., Li, Q., Shen, B., 2014. Mechanical properties and structural features of novel Fe-based bulk metallic glasses with unprecedented plasticity. Scientific Reports 4, 6233.

Yu, L., Wang, T.-C., 2017. Fracture Behaviors of Bulk Metallic Glasses Under Complex Tensile Loading. Journal of Applied Mechanics 85, 011003-011003-011006.

Yu, M.-h., 2002. Advances in strength theories for materials under complex stress state in the 20th Century. Applied Mechanics Reviews 55, 169-218.

Zhang, Z.F., Eckert, J., 2005. Unified Tensile Fracture Criterion. Physical Review Letters 94, 094301.

Zhang, Z.F., He, G., Eckert, J., Schultz, L., 2003. Fracture Mechanisms in Bulk Metallic Glassy Materials. Physical Review Letters 91, 045505.

Acknowledgments

The authors thank Dr. Cen Chen for her valuable help to revise our paper. This work was financially supported by the National Natural Science Foundation of China (Grant Nos. 11602272, 11602270, 11021262, and 11532013), the National Basic Research Program of China (”973” Project) (Grant No. 2012CB937500), and the Strategic Priority Research Program of the Chinese Academy of Sciences (Grant No. XDB22040503).

Competing financial interests: The authors declare no competing financial interests.

Figures captions

Figure 1. The stress state and fracture plane of round bar. (a) The round bar is subject to axial compression and superimposed confining pressure. The angle between the fracture plane and x_1-axis is θ. (b) The fracture plane and fracture angle are shown in the x_1-x_3 plane.

Figure 2. The critical fracture lines and critical Mohr circle under different deformation modes. The hyperbola is tangent to the critical Mohr circle at point A for pure shear strain and at point B for general case. The θ in the plot denotes the fracture angle and γ_{Cf} denotes the critical shear under general loading, while θ_0 and γ_{C0} represent the fracture angle and critical shear strain under pure shear strain respectively.

Figure 3. The critical fracture lines and critical Mohr circles for Vit-105 under different deformation modes. The gray line and green line are the fracture lines which represent pure strain ($\rho' = -1$) and general case ($\rho' = -0.5$) respectively. The blue line represents the case that radial strain is completely constrained ($\rho' = 0$). The critical Mohr circles are shown in different dash circles. The locus of tangency points is shown in the red line.

Figure4. The theoretical results of fracture strain (Vit-105). (a) Variations of the plastic strain $|\varepsilon_{11p}|$ and $|\varepsilon_{22p}|$ with ρ. (b) Variations of the elastic strain ε_{11e} and ε_{22e} with ρ. (c) Variations of the total fracture strain $|\varepsilon_{11}|$ and $|\varepsilon_{22}|$ with ρ. (d) The shear strain $\gamma/2$ at the fracture plane versus ρ.

Figure 5. The result of fracture angle (Vit-105). Variations of fracture angle θ

with respect to the proportionality coefficient ρ.

Figure 6. Critical shear strain vs. critical normal strain (along fracture plane). The six blue points represent the normal and shear strains under different loading modes ($\rho = -0.1, \ldots, 0.6$). The red line shows the fracture strains under different deformation modes.

Figure 7. Present analysis results vs. experimental data. The blue points are experimental data and the red line shows the present analysis results.

Figure. 8. Axial plastic fracture strain $|\varepsilon_{11p}|$ for various material constant β. With the increasing of β, the fracture changes from elastic failure (red line) to plastic failure (blue line). The basic parameters such as α, α_C, γ_{C0} are obtained from the experimental data of Vit-105.

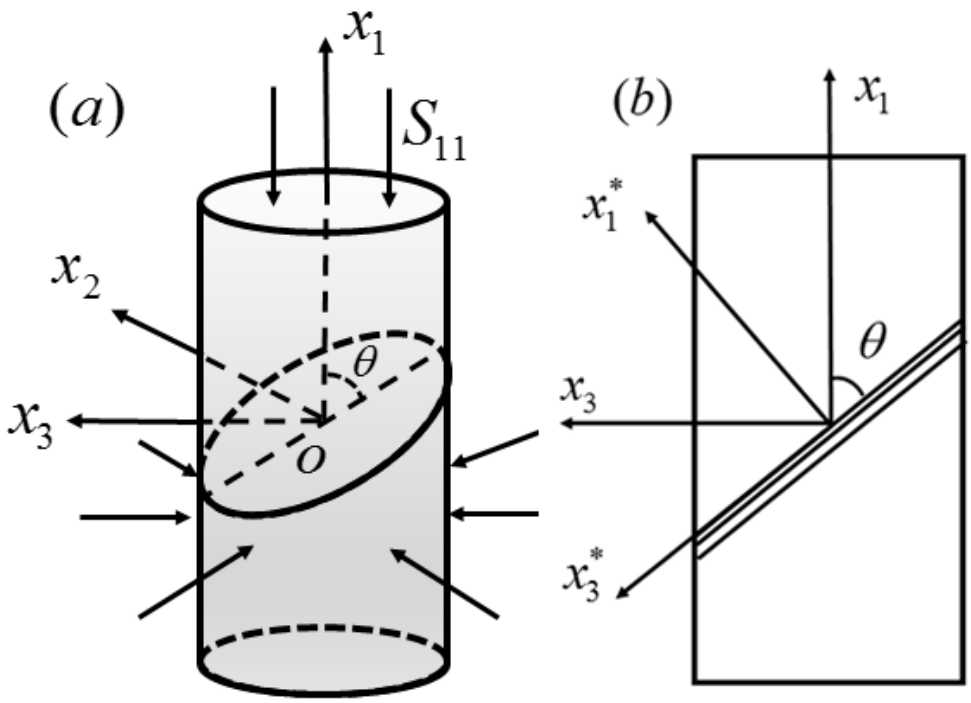

Figure. 1

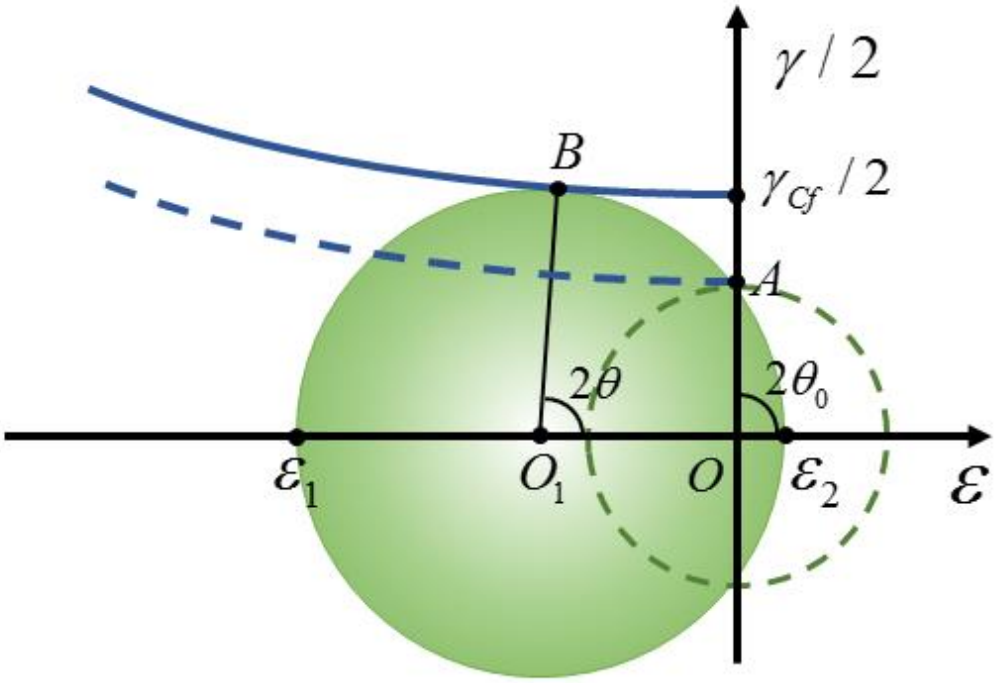

Figure. 2

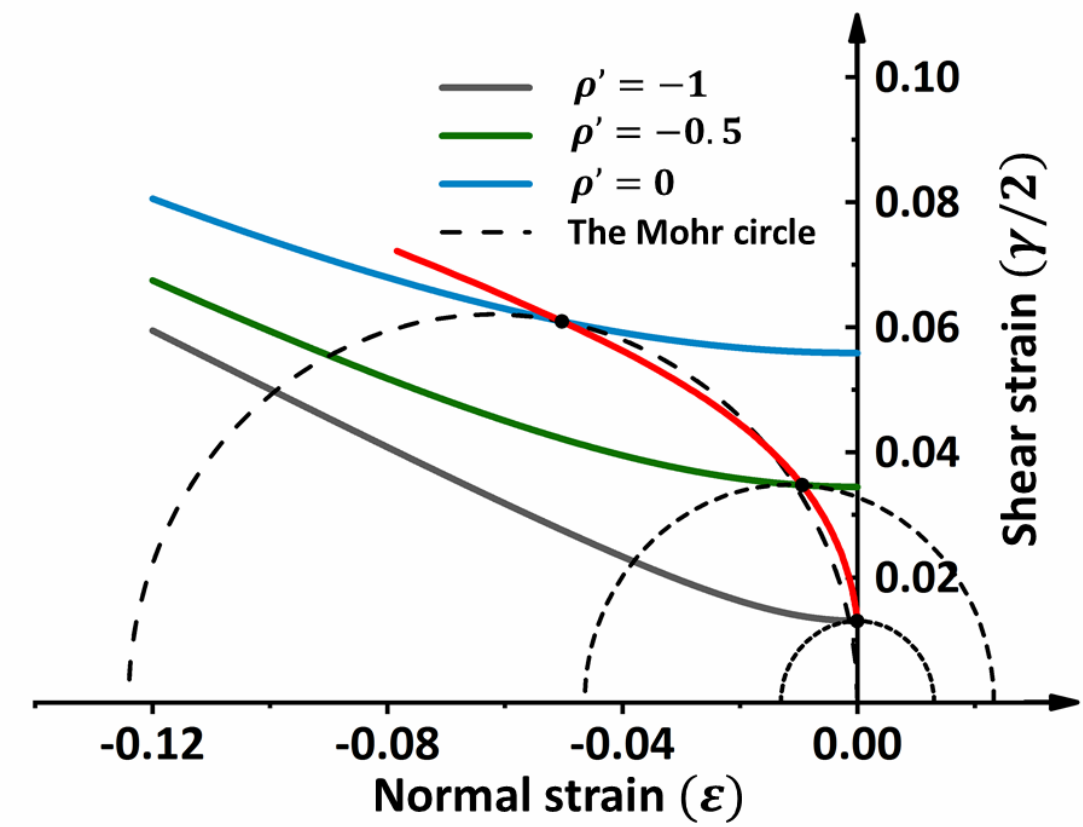

Figure. 3

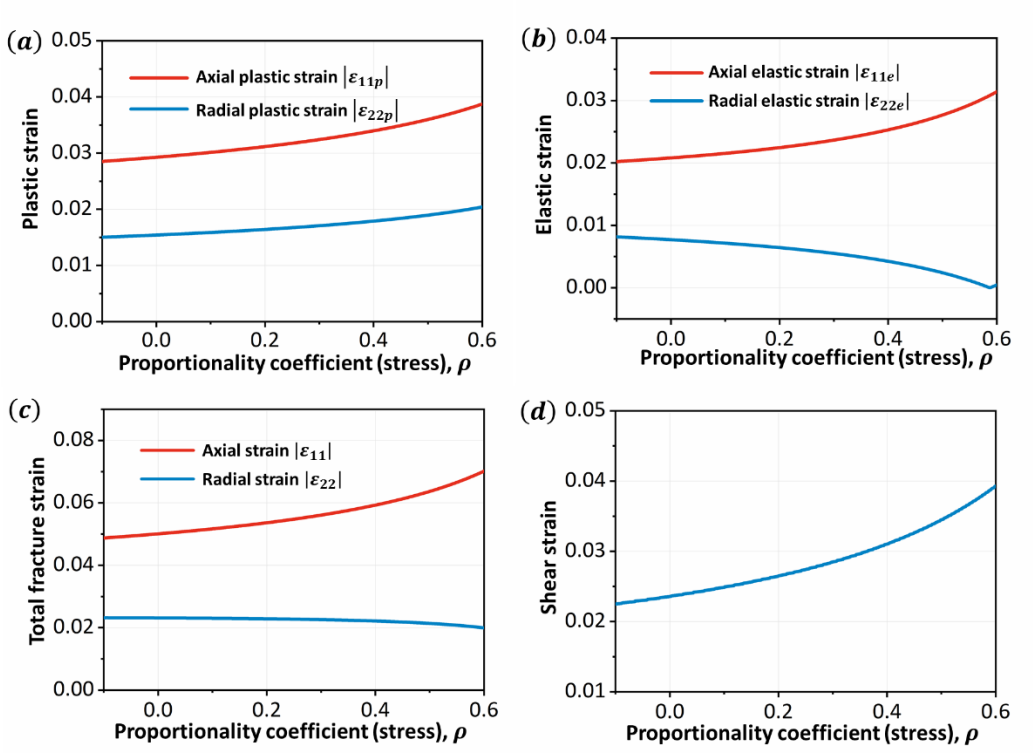

Figure. 4

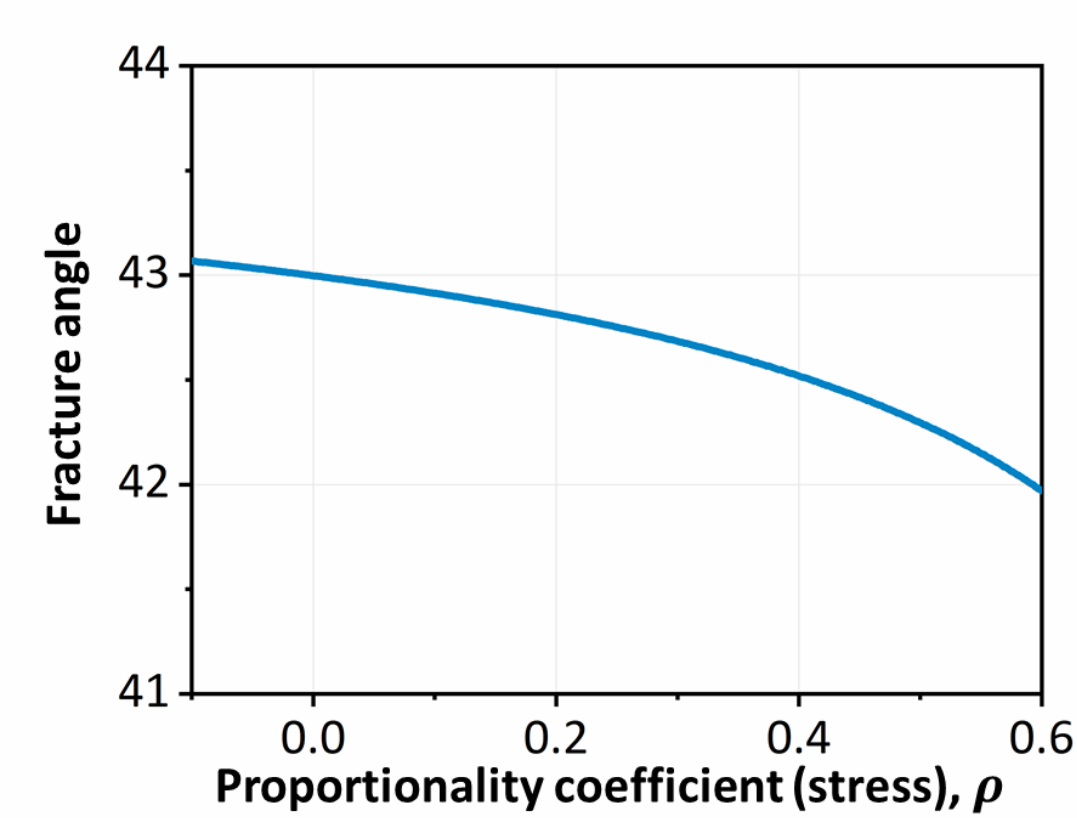

Figure. 5

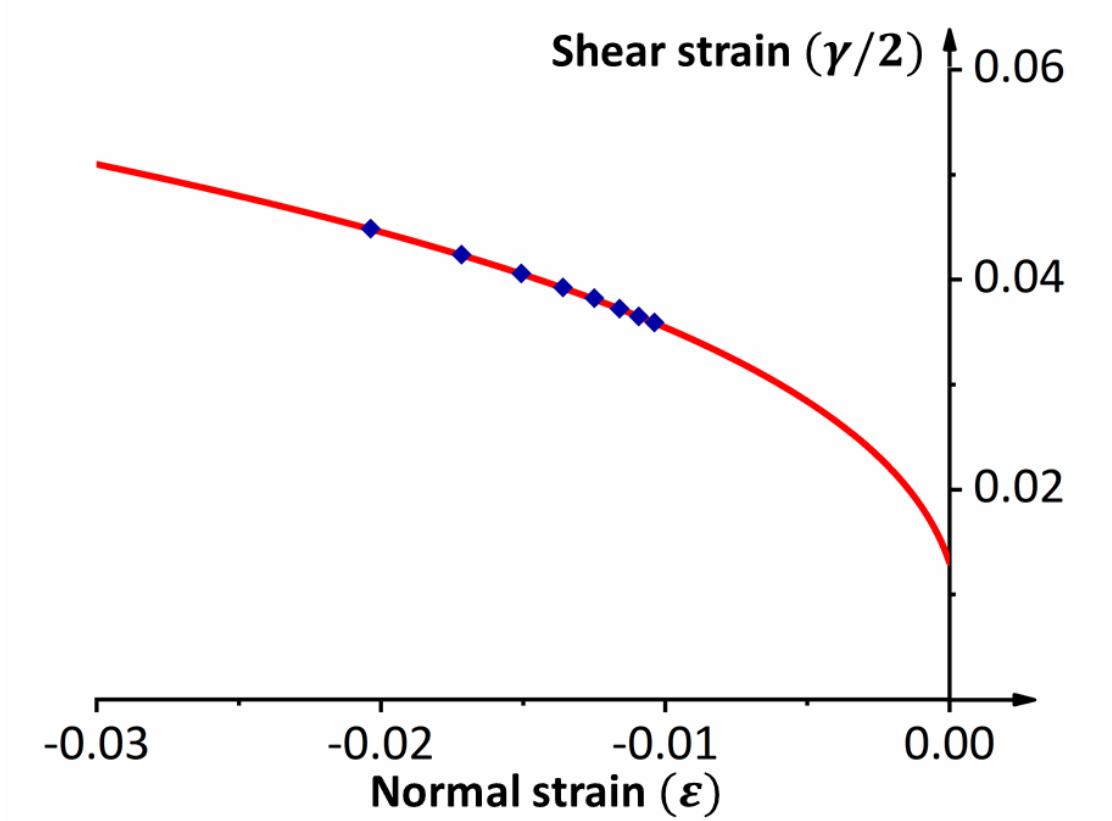

Figure. 6

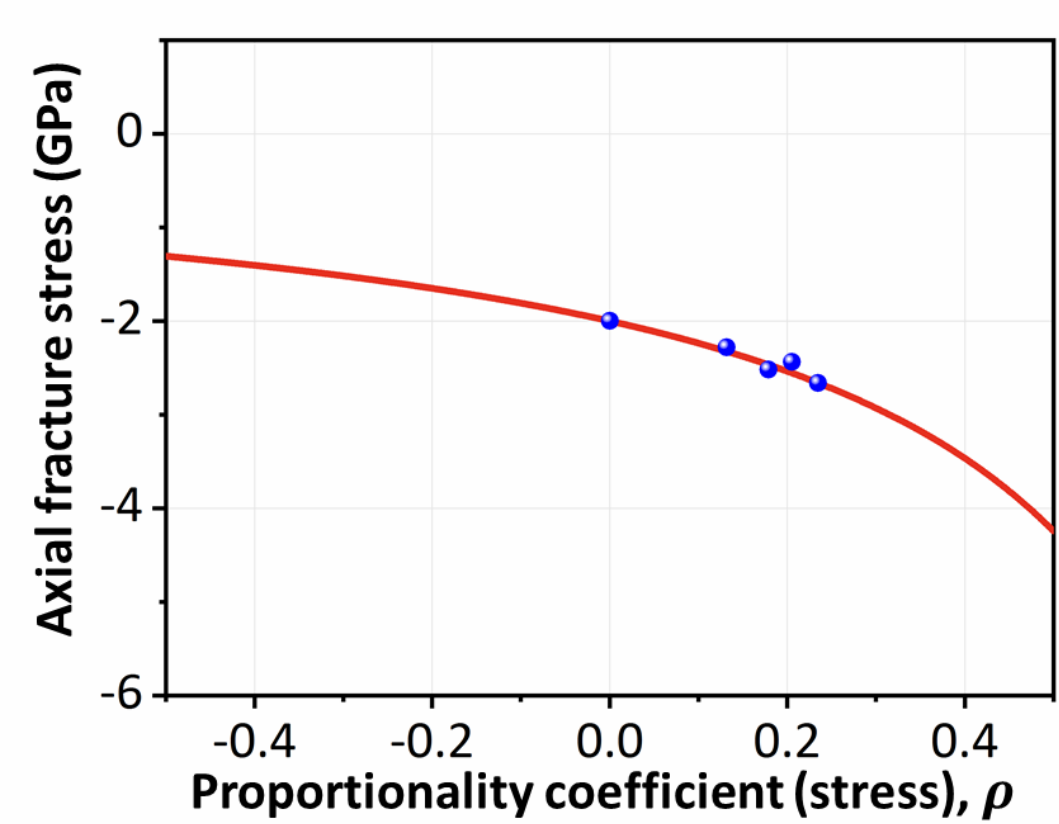

Figure. 7

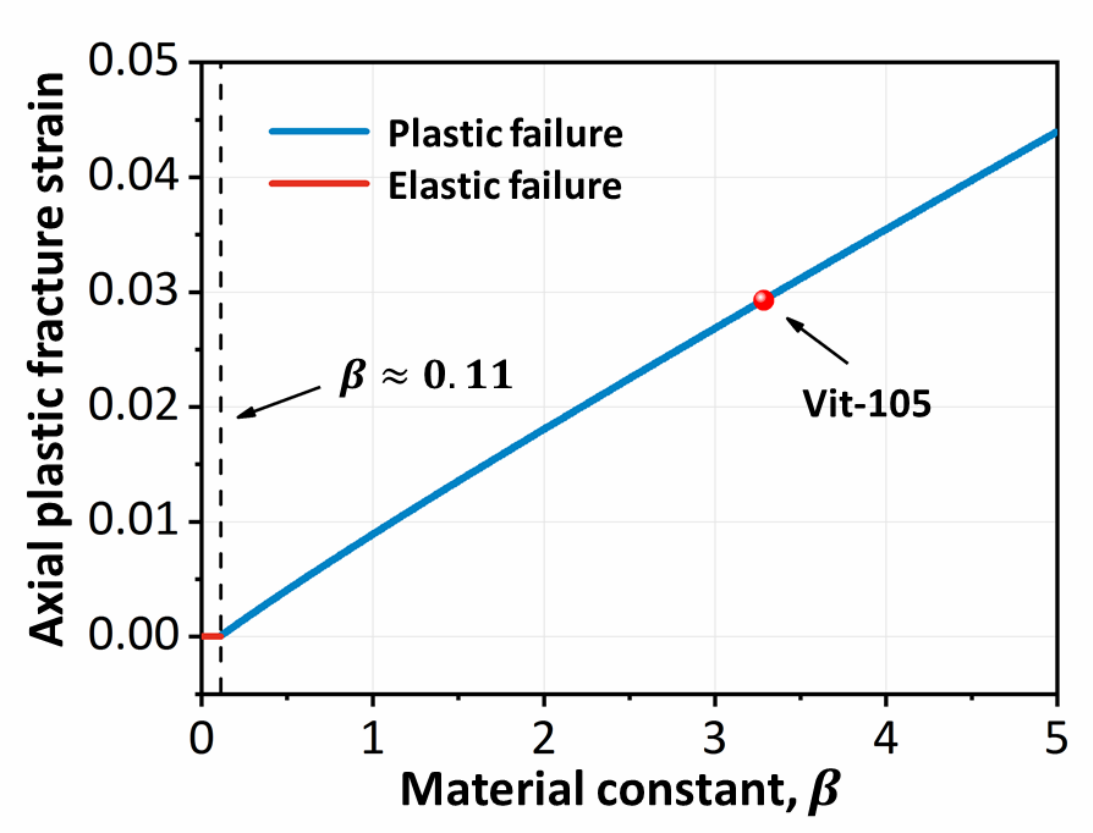

Figure. 8